ADVANCING EARTH AND SPACE SCIENCES

JGR Oceans

RESEARCH ARTICLE
10.1029/2024JC022094

Special Collection:
Regional Sea Level Change and Society

Key Points:

- Seafloor subsidence from present-day ice mass loss is as significant as glacial isostatic adjustment and is removed from altimeter data
- Relative sea level (RSL) change extrapolated from 2020 to 2050 ranges from 12 to 22 cm regionally with significant variation about the global mean
- Observation-based extrapolations produce significant overlap with climate-model projections of RSL change

Supporting Information:

Supporting Information may be found in the online version of this article.

Correspondence to:

A. Bellas-Manley,
ashley.bellas@colorado.edu

Citation:

Bellas-Manley, A., Nerem, R. S., & Hamlington, B. D. (2025). Extrapolation of the satellite altimeter record to understand regional variations in future sea level change. *Journal of Geophysical Research: Oceans*, *130*, e2024JC022094. https://doi.org/10.1029/2024JC022094

Received 14 NOV 2024
Accepted 2 MAY 2025

Author Contributions:

Conceptualization: A. Bellas-Manley, R. S. Nerem
Data curation: A. Bellas-Manley
Formal analysis: A. Bellas-Manley
Funding acquisition: R. S. Nerem
Investigation: A. Bellas-Manley, R. S. Nerem
Methodology: A. Bellas-Manley, R. S. Nerem, B. D. Hamlington
Software: A. Bellas-Manley
Supervision: R. S. Nerem, B. D. Hamlington
Validation: A. Bellas-Manley
Visualization: A. Bellas-Manley
Writing – original draft: A. Bellas-Manley

Extrapolation of the Satellite Altimeter Record to Understand Regional Variations in Future Sea Level Change

A. Bellas-Manley[1], R. S. Nerem[1,2], and B. D. Hamlington[3]

[1]Smead Department of Aerospace Engineering Sciences, Colorado Center for Astrodynamics Research, University of Colorado Boulder, Boulder, CO, USA, [2]Cooperative Institute for Research in Environmental Sciences, University of Colorado Boulder, Boulder, CO, USA, [3]Jet Propulsion Laboratory, California Institute of Technology, Pasadena, CA, USA

Abstract We perform a quadratic extrapolation of sea level on a regional scale based on satellite altimeter observations spanning 1993.0–2023.0, including corrections for natural climate variability, vertical land motion, and a rigorous assessment of the uncertainties associated with serially correlated formal errors, glacial isostatic adjustment, and satellite altimeter measurement errors. The extrapolations are data-driven and show the trajectory of relative sea level (RSL) over the last 30 years extrapolated into the future. These extrapolations suggest that RSL rise in 2050 relative to 2020 will be 22 ± 5 cm in the North Pacific, 19 ± 6 cm in the North Atlantic, 17 ± 4 cm in the South Atlantic, 15 ± 5 cm in the Indian Ocean, 14 ± 5 cm in the South Pacific, 13 ± 5 cm in the Tropical Pacific, and 12 ± 4 cm in the Southern Ocean. The regional results may differ from each other by more than 80% and differ significantly from the extrapolated global mean sea level rise of 16 ± 4 cm in most cases. The errors in these regional extrapolations are relatively narrow, and we show significant overlap with the regional projections from the most recent IPCC Sixth Assessment Report. The results provide an additional line of evidence when considering how representative the range of climate model projections are in describing near-term sea level rise and highlight the significance of regional variations in estimates of future sea level.

Plain Language Summary Satellite altimeters have measured a global map of the sea surface approximately every 5 days since 1993.0 (e.g., TOPEX/Poseidon, Jason-1, Jason-2, Jason-3, Sentinel-6 Michael Freilich). We use the 30-year record of observed sea level change to estimate the quadratic trajectory of sea level 30 years into the future, assuming that past changes will continue. We build upon previous research on global mean sea level by considering seven ocean-basin-scale regions. The altimeter data are corrected for natural climate variability and changes in the solid Earth. Until recently, it was not possible to perform quadratic extrapolations of regional sea level rise because large-scale modes of variability such as the El Nino Southern Oscillation imparted large periodic perturbations to the rate and acceleration. However, after 30 years of observation, the perturbations are starting to average out. We assess how much the rate and acceleration of sea level rise may change in the future with a rigorous assessment of the uncertainties associated with satellite altimeter measurement errors, GIA, and serially correlated formal errors. Ultimately, the data-driven extrapolations provide an independent estimate of future sea level and may aid in the selection of specific climate model projection scenarios (i.e., AR6-SSPs) in regional response strategies.

1. Introduction

The satellite altimeter record of sea level change is now more than 30 years in length, and the long-term climate-driven change (i.e., the forced response) is beginning to emerge in the data (Fasullo & Nerem, 2018; Richter et al., 2020). Recent work by Nerem et al. (2022) showed that the rate and acceleration of global mean sea level (GMSL) change have become steady against the addition of new altimeter data since 2017 (i.e., the rate and acceleration of GMSL do not change as data beyond 2017 is added to the record), and this may indicate that the observational record is now sufficiently long for the effects of interannual to decadal variability (e.g., the El Niño Southern Oscillation or ENSO, the Pacific Decadal Oscillation or PDO, etc.) to average out and reveal the forced response. An acceleration in the forced response of sea level is expected based on climate model projections like the Sixth Assessment Report from the IPCC (i.e., the AR6; Fox-Kemper et al., 2021b), observed increases in ice mass loss rates (e.g., Diener et al., 2021; Hugonnet et al., 2021; Velicogna et al., 2020), and is confirmed by the accelerating GMSL time series from satellite altimetry (Nerem et al., 2022). These changes in GMSL provide an important indicator of the changing climate, integrating the combined effects of the warming ocean, atmosphere, and

Writing – review & editing: A. Bellas-Manley, R. S. Nerem, B. D. Hamlington

cryosphere and have been used to estimate the near-term trajectory of sea level rise and how it compares to model-based projections (e.g., Fox-Kemper et al., 2021b; Nerem et al., 2022). Beneath the global scale change, however, there are significant variations in the magnitude and pattern of sea level change on regional scales (e.g., Hamlington et al., 2020; Jevrejeva et al., 2014; Slangen et al., 2014; Sweet et al., 2017). In the following study, we assess the regional variations in sea level change based on the 30-year satellite altimeter record and compare with climate model projections.

Sea level change varies on a regional scale because of spatial variations in the distribution of mass and density changes in the oceans. The drivers of sea level change include ice sheets, glaciers, and terrestrial water storage (i.e., mass change), thermosteric changes (i.e., density change), and the redistribution of these mass and density changes from gravitational, rotational, and deformational effects (GRD), ocean dynamics and circulation, GIA and other processes (e.g., Fox-Kemper et al., 2021b; Ishii et al., 2006; Kopp et al., 2015; Mitrovica et al., 2001; Peltier et al., 2015; Stammer et al., 2013). Moreover, regional changes in sea level and its gradients are an important driver and indicator of changes in surface ocean currents including the Antarctic Circumpolar Current and western boundary currents such as the Gulf Stream. Regional variations in the rate and acceleration lead to significantly different changes in estimates of future sea level from one region to another and are therefore important to consider. However, considering sea level on a regional rather than global scale introduces additional challenges and complexities. For example, the natural variations that cause sea level to change on interannual to decadal timescales can be much larger on regional compared to global spatial scales. A longer observation period is thus required for the impact of interannual to decadal variability to average out and reveal the long-term signal in sea level rise when smaller spatial scales are considered. Special care is taken to separate the long-term, climate-change driven trends from internal variability in the following work.

In this study, we seek to answer the following questions: (a) can the long-term rate and acceleration of sea level rise be extracted from the 30-year satellite altimeter record on a regional scale? (b) how large are the uncertainties in the regional sea level rise signals? (c) by how much do the regional quadratic extrapolations differ from each other, from the global mean, and how do they compare with climate-model projections? Our work is motivated by the need for additional lines of evidence to support adaptation and mitigation to sea level change in coastal regions. We present (a) quadratic extrapolations of satellite altimeter observations on a regional scale, (b) a rigorous assessment of the uncertainties, and (c) a self-consistent comparison between corrected altimeter data and climate model projections.

2. Observations and Methods

The Jet Propulsion Lab MEaSUREs Gridded Sea Surface Height Anomalies Version 2205 provides a continuous record of sea surface height across the global oceans from multiple satellite altimeter missions spanning 1993.0 to 2023.0 at smoothed five-day intervals (TOPEX/Poseidon, Jason-1, Jason-2, Jason-3, and Sentinel 6) (Fournier et al., 2022). We consider the MEaSUREs data on a $0.33° \times 0.33°$ spatial grid and apply a monthly average as well as corrections for long-term sources of vertical land motion (VLM; see Section 2.1) and internal variability (see Section 2.2). Then, from this corrected record, we calculate the rate and acceleration in RSL at each coordinate (Figure 1) and in ocean basin-scale regions to produce regional extrapolations (presented later). We define the rate and acceleration following

$$f(t) = b + rt + \frac{1}{2}at^2 \tag{1}$$

where b is the bias, r is the rate, and a is the acceleration.

2.1. Vertical Land Motion From GIA and Present-Day Ice Mass Loss

Satellite altimeters measure geocentric sea level (GSL), which is the height of the sea surface relative to a fixed reference frame (e.g., the mean sea surface in the case of the MEaSUREs data) (Gregory et al., 2019; Tamisiea, 2011). Climate model projections, on the other hand, are generally presented in terms of RSL, which is the height of the sea surface relative to the sea floor (e.g., the IPCC AR6; Fox-Kemper et al., 2021b, Table 9.7). Since a primary aim of the present study is to draw comparison between observation-based extrapolations and climate

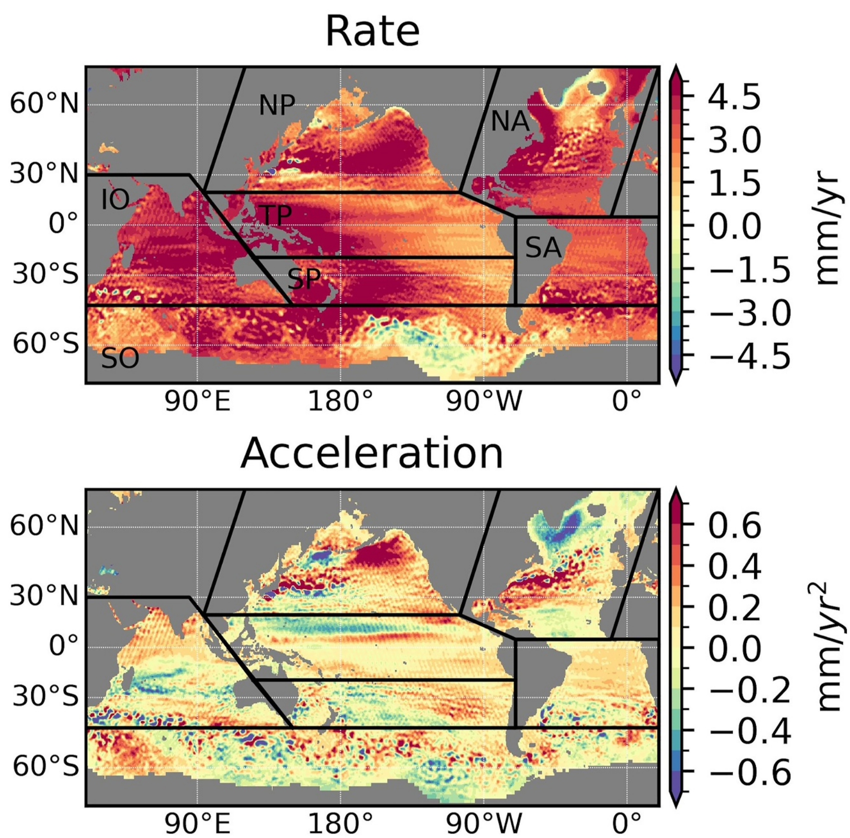

Figure 1. The rate (top) and acceleration (bottom) of relative sea level based on the MEaSUREs Gridded Sea Surface Height Anomalies Version 2205, corrected for (i) vertical land motion driven by glacial isostatic adjustment and present-day ice mass loss (Section 2.1), and (ii) internal variability following the cyclostationary empirical orthogonal function technique (Section 2.2). Regions are abbreviated as IO (Indian Ocean), SO (Southern Ocean), NP (North Pacific), TP (Tropical Pacific), SP (South Pacific), NA (North Atlantic), and SA (South Atlantic).

model projections, we apply a correction for VLM to the altimeter record of GSL to convert GSL to RSL (Frederikse et al., 2017; Gregory et al., 2019; Riva et al., 2017; Tamisiea, 2011; Vishwakarma et al., 2020),

$$\mathrm{RSL}(t,\theta,\varphi) = \mathrm{GSL}(t,\theta,\varphi) - \mathrm{VLM}(t,\theta,\varphi) \tag{2}$$

where t is time, θ is latitude, and φ is longitude.

The only difference between GSL and RSL is the reference frame relative to which they are measured, such that converting GSL to RSL requires a simple reference frame transformation, which is accomplished by subtracting the motion of the sea floor (i.e., VLM). Climate model projections in the AR6 consider changes in RSL driven by eight contributing processes: (a) the Greenland ice sheet (GrIS), (b) the Antarctic ice sheet (AIS), (c) glaciers, (d) terrestrial water storage, (e) thermal expansion, (f) ocean dynamics, (g) GRD, and (h) GIA plus other sources of long-term VLM. In terms of GSL, the shape of the sea surface is also controlled by these eight contributing sources identically to RSL except it is measured relative to a fixed reference rather than a deformable one. To convert GSL from satellite altimeters to RSL as consistently with the climate models as possible, we consider VLM driven by GIA based on ICE-6G*VM5a (Peltier et al., 2015) and VLM driven by the ongoing GRD response to present-day ice mass loss at GrIS, AIS, and glaciers. This calculation accounts for the primary drivers of VLM, although we acknowledge that the climate models also include VLM from tectonics, subsidence due to groundwater and hydrocarbon withdrawal, and sediment compaction. However, since these have fairly short wavelengths and averaging is applied across basin-scale regions in the present work, we neglect these sources of VLM.

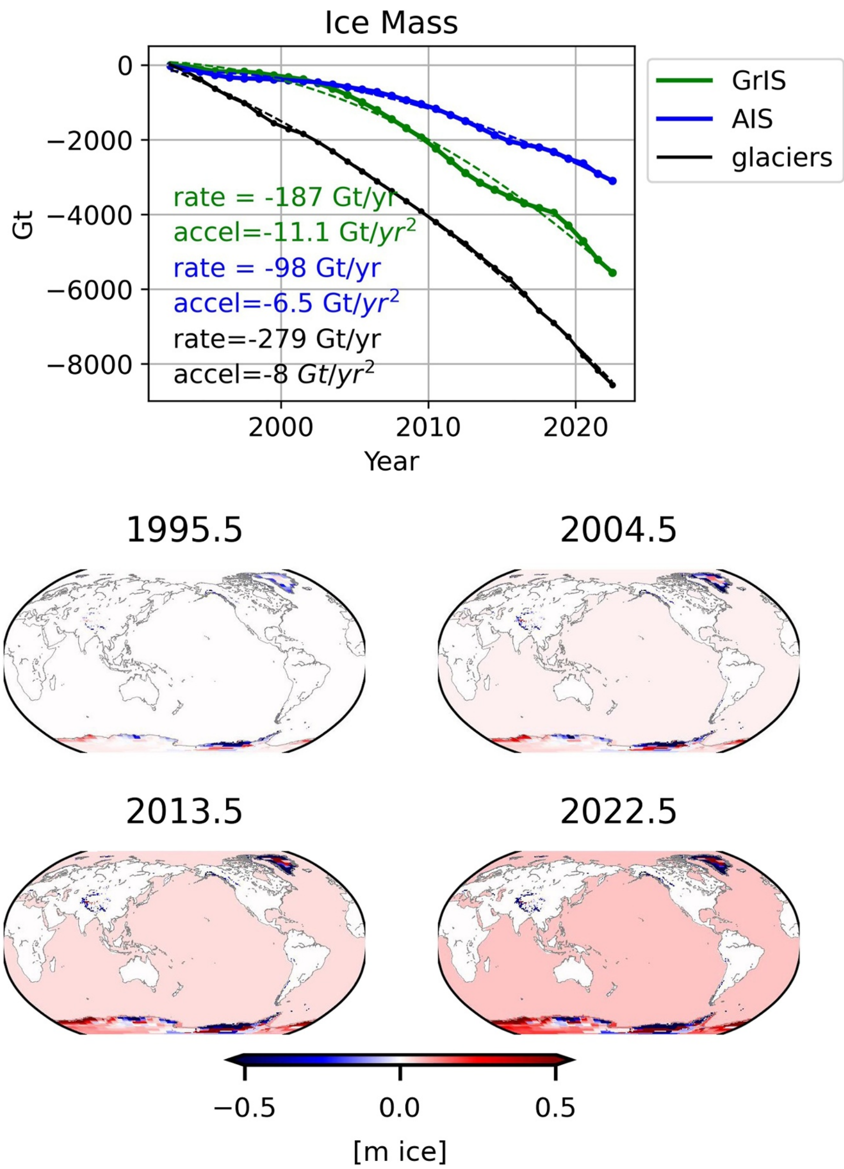

Figure 2. The surface loading history driven by ice mass loss at the Greenland ice sheet, Antarctic ice sheet, and global glaciers from 1993 to 2023. The rates superposed on the upper panel are solved at the mean time of the timeseries (2008).

We compute the ongoing GRD response including VLM to present-day ice mass loss at GrIS and AIS based on the IMBIE data (Otosaka et al., 2023 and references therein). The IMBIE data are an ideal choice for ice sheet mass loss because (a) it extends across most of the altimeter era, and (b) it incorporates observations from multiple remote sensing missions including GRACE, GRACE-FO, ICESat-1, ICESat-2, and CryoSat-2 as well as three independent methods for estimating mass change (e.g., altimetry, gravimetry, and the input-output method). We average the IMBIE data onto annual time steps, 1992.5–2020.5, and then extrapolate quadratically onto 2021.5 and 2022.5 to cover the full time period of the altimeter record. Over this time period, the rate and acceleration of ice mass loss at GrIS are −187 Gt/year and −11.1 Gt/year^2, respectively, and at AIS, −98 Gt/year and −6.5 Gt/year^2 (Figure 2). Because IMBIE provides timeseries data for GrIS and AIS but not a spatiotemporal data set, we distribute the ice mass loss over Greenland and Antarctica based on a normalized trend map of the JPL GRACE mascons (Wiese et al., 2023) (Figure 2). The static ocean load is computed based on the ice mass loss on land, uniformly distributed across the global oceans, and added to the loading history.

To compute the GRD response to present-day ice mass loss at GrIS and AIS, the loading history is convolved with the viscoelastic structure of the Earth. The solution computes the perturbations in the geoid, rotation axis, and deformation of the solid Earth surface and thus updates the static ocean load to include a dynamic ocean load (i.e., nonuniform sea surface height that conforms to the geoid). The solution is time-dependent because the ice mass loss is accelerating, and time steps are annual spanning 1992.5–2022.5. The density and elastic structure of the Earth is based on the preliminary reference Earth model, viscosity is based on VM5a (Peltier et al., 2015) and further details of the semianalytic model used to compute the ongoing GRD response to present-day ice mass loss are described by Paulson et al. (2005) and A et al. (2013).

The ongoing GRD response to ice mass loss from glaciers is computed similarly to that from GrIS and AIS. However, the surface mass loading history for glaciers is derived from the dynamic glacier evolution model PyGEM (Rounce et al., 2023) rather than satellite observations because the very small spatial scale of glaciers renders them difficult to observe (e.g., a significant proportion of glaciers are on the order of 1–100 km^2). We consider glaciers in all 20 regions of the Randolph Glacier Inventory, including the peripheral glaciers of GrIS and AIS, which are neglected in the IMBIE data set. Monthly solutions of glacier mass evolution are interpolated onto a $0.5° \times 0.5°$ resolution grid and averaged annually 1992.5–2022.5 over which the global glacier mass loss rate and acceleration are −279 Gt/year and −8 Gt/year^2, respectively (Figure 2).

Significant VLM is driven by both GIA and present-day ice mass loss (Figure 3). Although it is common practice to correct satellite observations for GIA to isolate changes in the ocean, VLM driven by present-day ice mass loss is often ignored. We suggest that future studies of RSL based on satellite observations should consider correcting for VLM driven by present-day ice mass loss to more accurately isolate the redistribution of water-mass from deformation of the solid Earth in altimeter observations. Note that this includes studies of GMSL, which are generally based on altimeter observations corrected for GIA (e.g., Hamlington et al., 2024) but often fail to account for the VLM effects of present-day ice mass loss. The importance of VLM driven by present-day ice mass loss was previously noted by Riva et al. (2017), Frederikse et al. (2017), and Vishwakarma et al. (2020).

Ultimately, the calculation of VLM from present-day ice mass loss plus GIA (Peltier et al., 2015) is used to convert the altimeter record of GSL to RSL. The spatiotemporal VLM field is expanded from spherical harmonic coefficients ($l_{\max} = 100$) onto the MEaSUREs grid coordinates, interpolated onto monthly timestamps, and then subtracted from the MEaSUREs data prior to computing the rates and accelerations used in the extrapolations. This methodology preserves the effect of nonlinear time-dependence of ongoing GRD on the observations from altimetry.

2.2. Natural Climate Variability and the CSEOF Technique

We apply cyclostationary empirical orthogonal functions (CSEOFs) to identify and remove natural climate variability from the MEaSUREs data (e.g., Hamlington et al., 2019; Strassburg et al., 2014). The CSEOF decomposition of the MEaSUREs data produces CSEOF modes, which are comprised of a principal component time series (PCTS) and a set of maps (i.e., loading vectors or LVs). Each mode represents a specific amount of the variance in the original data set, where the first three modes combined explain 40% of the variance (Figure S1 in Supporting Information S1). To reconstruct the component of the original data set that is captured by a single CSEOF mode, the PCTS is multiplied with the loading vector (Figures S2–S4 in Supporting Information S1) (Hamlington et al., 2011).

The CSEOF modes are much like EOF modes with one important difference: in the CSEOF technique, the LV varies periodically in time (e.g., Hamlington et al., 2011). The benefit of the CSEOF technique is that each mode can capture periodic variability in the spatial pattern, which is particularly well-suited to capturing the behavior of internal modes of variability in the climate system. We set the nested period equal to 2 years to capture ENSO and PDO, which have previously been separated into biennial and decadal modes and account for a significant amount of the variance in the data (Hamlington et al., 2016). Since we apply a monthly average to the MEaSUREs data and a two-year nested period in the CSEOF decomposition, the CSEOF decomposition produces 24 spatial maps per mode.

Mode 1 captures the largest amount of variance in the original data set and represents the modulated annual cycle consistent with previously published work (e.g., Hamlington et al., 2011, 2014, 2019). This is also suggested by (a) the GMSL signal and (b) the fact that the maps for the first and second January in the loading vector look identical and similarly for other months (Figure S2 in Supporting Information S1).

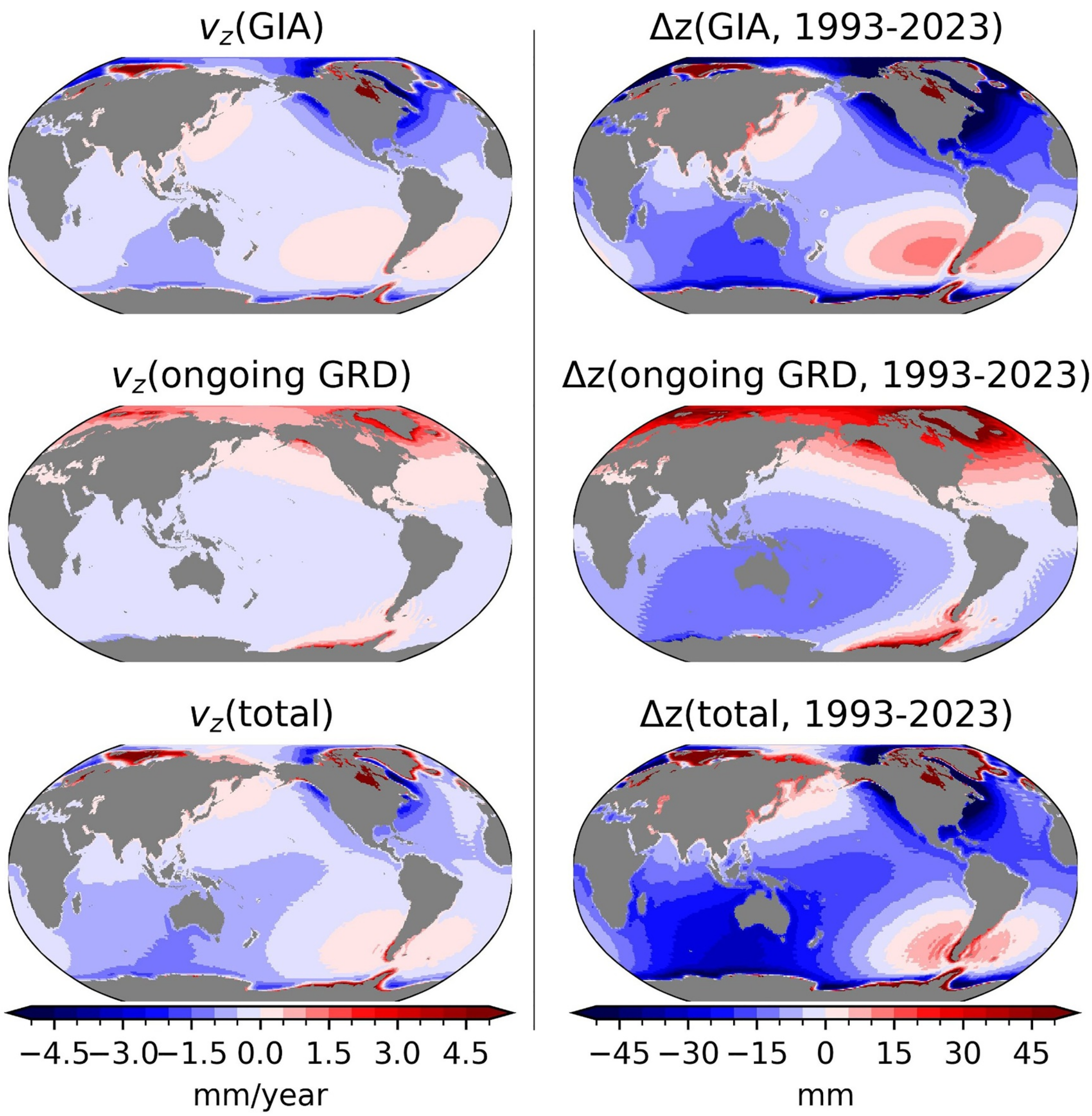

Figure 3. The vertical land motion component of the GRD response to surface loading associated with glacial isostatic adjustment (top row), present-day ice mass loss (middle row), and the sum of the two (bottom row) in terms of the vertical velocity, v_z (left column), and the accumulated total vertical displacement Δz over the time period 1993–2023 (right column). Note that v_z from ongoing GRD is nonlinear, and we present the average in time, 1993–2023, here.

Mode 2 and Mode 3 explain similar amounts of variance in the data and therefore appear to be coupled (Figure S1 in Supporting Information S1). Based on previously published work and the amplitude of the loading vectors in the Tropical Pacific and North Pacific, Mode 2 and Mode 3 are likely related to ENSO and the PDO (Figures S3 and S4 in Supporting Information S1). Beyond Mode 3, the modes are not well-separated in terms of the variance they explain and are considered poorly resolved (Figure S1 in Supporting Information S1). Therefore, we remove Mode 1, Mode 2, and Mode 3 from the MEaSUREs data to reduce the effects of internal variability in the observations. For a detailed description of the efficacy of the CSEOF technique at isolating the effects of internal variability associated with ENSO and PDO, refer to Hamlington et al. (2014).

3. Results

We present the MEaSUREs data corrected for VLM and natural climate variability averaged within seven large regions: the Indian Ocean, North Pacific, Tropical Pacific, South Pacific, North Atlantic, South Atlantic, and the Southern Ocean (Figure 4). Averaging the data into seven large regions demonstrates that it is generally well-fit by a quadratic, where the acceleration in regional RSL is particularly important to the fit in the North Pacific and

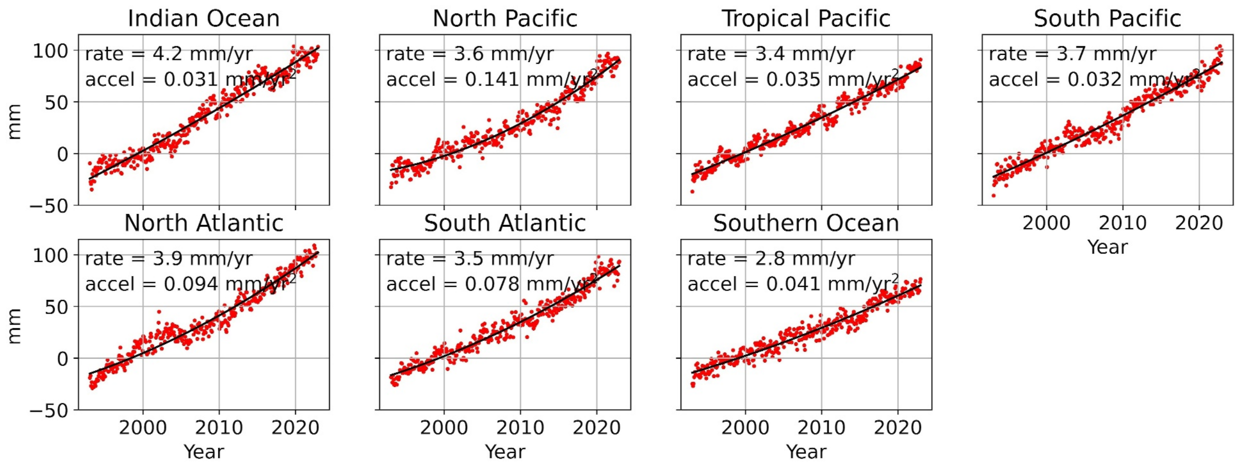

Figure 4. The MEaSUREs data corrected for vertical land motion driven by glacial isostatic adjustment and ongoing GRD, natural climate variability, and averaged into seven ocean basin-scale regions. A quadratic is fit to the data in which the rate is fit at $t_0 = 2008$ (the midpoint of the record).

the North Atlantic. We fit the rate and acceleration using linear least squares applied to Equation 1 plus annual and semiannual terms, and the regions are illustrated in Figure 1.

We assess the stability of the regional rates and accelerations based on the MEaSUREs data corrected for VLM and internal variability. We estimate the regional rates and accelerations based on a varying observation period on the basis that they will approach steady state as the interannual to decadal variability averages out to reveal the long-term signal (Figure 5) (Haigh et al., 2014). We assess the stability of the rate and acceleration as new data are added to the altimeter record: (a) to investigate whether a steady state has emerged on a regional scale and (b) to understand how much the extrapolations may change as more data is added to the record in the future.

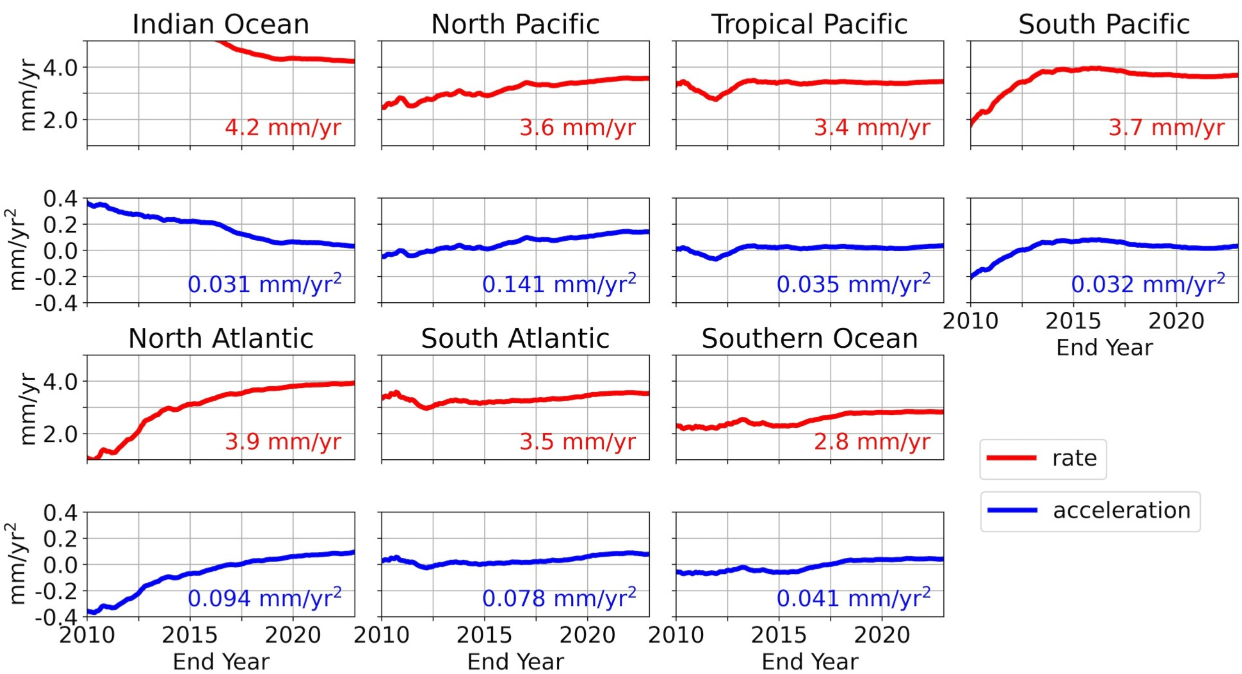

Figure 5. The regional rate and acceleration based on corrected satellite altimeter data spanning 1993.0 to a variable end year (shown on the horizontal axis). Rates are solved at $t_0 = 2008$, which is the midpoint of the complete data record spanning 1993.0–2023.0. The values of the rate and acceleration based on the complete data record are annotated on each panel.

The regional rates and accelerations are sensitive to the addition of new data prior to the year ∼2020. However, as the observational record is extended, the results approach steady values in most of the regions considered, indicating that the effects of interannual to decadal variability have begun to average out on a regional scale. In regions where the acceleration approaches a relatively large value, the rate continues to increase as expected. The results provide an indication of how much the quadratic extrapolations may change in the future. Average rates in the Indian Ocean, North Pacific, Tropical Pacific, South Pacific, North Atlantic, South Atlantic, and Southern Ocean approach steady values of 4.2 mm/year, 3.6 mm/year, 3.4 mm/year, 3.7 mm/year, 3.9 mm/year, 3.5 mm/year, and 2.8 mm/year, respectively. Accelerations in the same regions approach steady values of 0.03 mm/year^2, 0.14 mm/year^2, 0.04 mm/year^2, 0.03 mm/year^2, 0.09 mm/year^2, 0.08 mm/year^2, and 0.04 mm/year^2, respectively.

Sterodynamic changes control the regional variations we observe, whereas mass-driven or manometric changes (Gregory et al., 2019) are much smoother and larger in scale (Figure 1; e.g., Adhikari et al., 2016). A possible driver of the moderate to large positive accelerations observed in the North Atlantic (0.094 mm/yr^2), the North Pacific (0.141 mm/yr^2), and the South Atlantic (0.078 mm/yr^2) is the increasing strength of the western boundary current (e.g., Gulf Stream) and corresponding expansion of the tropics that arises in response to climate change (Seager & Simpson, 2016; Yang et al., 2016, 2020). Although recent work has shown that the strong positive acceleration in the U.S. Southeast Coast and Gulf Coast represents the compounding effects of the forced response and natural climate variability (Dangendorf et al., 2023; Zhang et al., 2024), the bimodal pattern of acceleration in the mid- and far-North Atlantic closely projects onto the subtropical and subpolar gyres, which produce sterodynamic sea surface highs and lows, respectively (Karnauskas, 2020). Therefore, we suggest that the strong negative acceleration in the far-North Atlantic may be controlled similarly to that in the U.S. Southeast and Gulf Coast, such that the average over the North Atlantic in total may not necessarily be biased high by natural climate variability. Furthermore, strengthening of the subtropical and subpolar gyres may have implications for the Atlantic Meridional Overturning Circulation but this bimodal pattern is not clearly discerned in the trend pattern of the North Atlantic and warrants further investigation when longer timeseries observations are available.

The relatively low acceleration observed in the Tropical Pacific (0.035 mm/yr^2) is partially the result of strong zonal bands of positive and negative accelerations, which cancel each other between ∼0°N and ∼20°N and are consistent with strengthening of the North Equatorial Current and the North Equatorial Counter Current, both of which are geostrophic currents driven by tropical trade winds (e.g., Karnauskas, 2020). This result is particularly interesting given the uncertainties surrounding the response of the Tropical Pacific mean state to climate change, which is also linked to the tropical trade winds, where historical records indicate strengthening of the zonal gradient in key variables such as SST consistent with the satellite altimeter observations considered here, whereas climate models predict weakening of the zonal gradient associated with enhanced warming in the eastern equatorial Pacific (Lee et al., 2022).

The Antarctic overturning circulation weakened significantly between 1994 and 2018 (Gunn et al., 2023), which may reduce the rate at which warmer equatorward waters are pulled into the circumpolar current and may explain the relatively low acceleration in sea level rise that we observe in the Southern Ocean (0.041 mm/yr^2). The weak acceleration in the South Pacific (0.032 mm/yr^2) indicates that the western boundary current is relatively steady despite global climate change.

Finally, although the acceleration in the Indian Ocean is weak on average, it is strong and positive in the north where northward transport is blocked by the Eurasian continent. Meanwhile, the South Indian Ocean may exchange heat and mass with the Southern Ocean possibly explaining the deceleration of sea level rise observed there (Dalpadado et al., 2024; Ummenhofer et al., 2021). This bimodal pattern maps onto the Indian Ocean gyre but is approximately orthogonal to the dominant mode of natural climate variability in the region, the Indian Ocean Dipole, which has an east-west gradient and, furthermore, is coupled to the ENSO mode in the CSEOF decomposition and is partially removed with it (Figure S3 in Supporting Information S1).

3.1. Error Analysis

Uncertainties are quantified following the methods of Maul and Martin (1993) to account for the lag-1 serial correlation of the formal errors, which are enhanced by the interannual and decadal variability that remains in the data (Bos et al., 2014; Royston et al., 2018). Errors associated with GIA are estimated based on a 5000-member ensemble of GIA models from a Bayesian inversion that considers both varying ice loading histories and

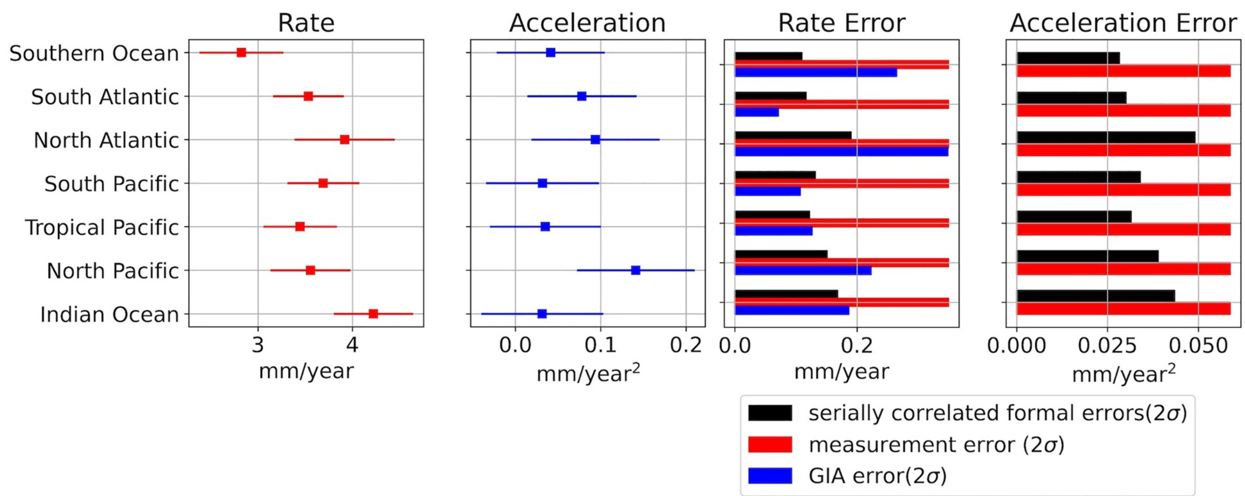

Figure 6. (Left) The rate and acceleration of relative sea level rise with error bars representing the composite 2**σ** confidence limit based on a Monte Carlo simulation of measurement errors, serially correlated formal errors, and glacial isostatic adjustment, and (right) the 2**σ** error sources that contribute to the composite uncertainties.

viscoelastic Earth structures (Caron et al., 2018). We compute the average VLM response in each region and each member of the GIA model ensemble, then take the standard deviation across members to estimate the error. The uncertainty in GIA-driven VLM is the appropriate quantity to consider since this is what is removed from the altimeter data (i.e., to convert GSL to RSL). Finally, measurement errors are assumed to be uniform across the global oceans and modeled based on each potential error source, including altimeter noise, geophysical corrections, orbit determination, wet troposphere corrections, precision orbit determination, intermission biases, large-scale drifts associated with reference frame uncertainties, and the instabilities of TOPEX/Poseidon (Ablain et al., 2019; Nerem et al., 2022). The errors from all of these sources are modeled in a Monte Carlo simulation with 10,000 members from which confidence limits are estimated.

The Monte Carlo simulation is performed by constructing normal distributions with mean equal to zero and standard deviation equal to the 1-sigma rate-error or 1-sigma acceleration-error associated with each potential error source (shown by the histogram-style bar plot in Figure 6). We randomly sample from the normal distribution of each error source and then add the sum of these samples to the best-fit rate or acceleration 10,000 times. The bounds within which 95% of the simulation members lay defines the composite 2-sigma error (shown by the box-and-whisker plot in Figure 6).

Based on the composite uncertainty associated with random perturbations from serially correlated formal errors, GIA, and measurement errors (Figure 6), the regional rate of sea level rise is statistically significant in all of the regions considered. Regional accelerations, on the other hand, are statistically significant in the South Atlantic, North Atlantic, and North Pacific, but not the Southern Ocean, South Pacific, Tropical Pacific, nor Indian Ocean (Figure 6). Regarding the rate uncertainty, serially correlated formal errors generally account for 15%–24% of the total error, errors associated with GIA account for 13%–39% of the total error and measurement errors account for 39%–65% of the total error (Figure 6). Regarding the acceleration uncertainty, measurement errors and serially correlated formal errors contribute 54%–68% and 32%–43%, respectively, and GIA contributes no error because there is no known acceleration associated with GIA at present-day. A longer observational record will help to reduce both the serially correlated formal errors (e.g., as interannual to decadal variability average out to greater degree) and the measurement errors (e.g., as increasingly sophisticated satellite altimeter missions are launched and improvements to postprocessing techniques are made). Improvements to GIA modeling is also an active area of research (e.g., Gomez et al., 2024).

3.2. Data-Driven Extrapolations

The regional rates and accelerations are fit along with annual and semiannual terms and $t_0 = 2008$ (the midpoint of the time series) using linear least squares applied to the MEaSUREs data corrected for VLM and internal variability (Figure 4). The results are then used to produce regional quadratic extrapolations of RSL from 2020 to

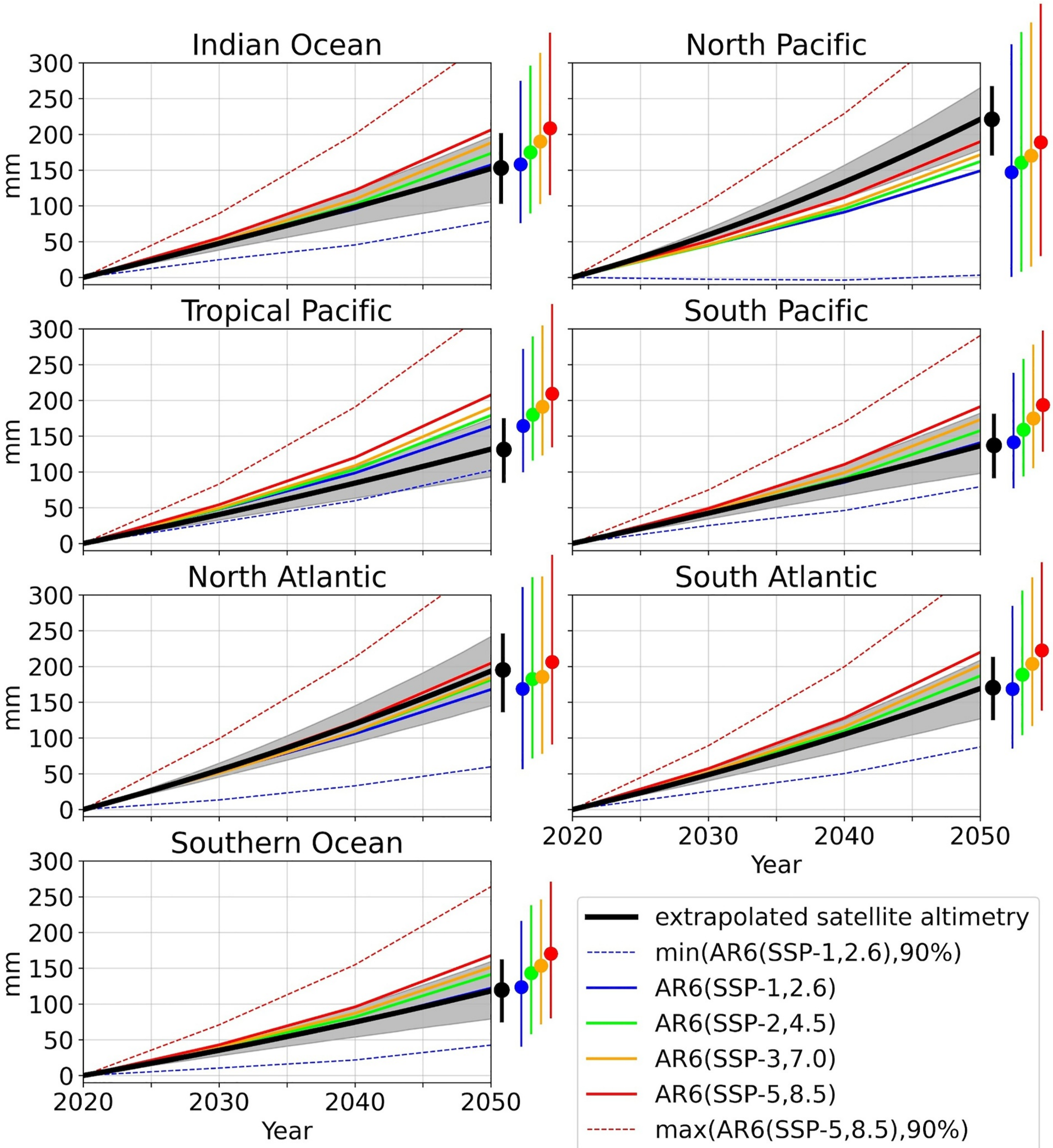

Figure 7. Quadratic extrapolations of relative sea level (RSL) based on the satellite altimeter record corrected for vertical land motion (VLM) and internal climate variability in seven ocean basin-scale regions with 90% confidence limits (black line and shading). Colored lines show the IPCC AR6 climate model projections of RSL based on various shared socio-economic pathways or emissions scenarios, including the summed effects of glaciers, ice sheets, terrestrial water storage, thermosteric changes, ocean dynamics and circulation, glacial isostatic adjustment plus long-term sources of VLM, and GRD. Dashed lines show the 90% confidence limits based on FACTS (Kopp et al., 2023). The whiskers show the 90% confidence limits for the corrected altimeter data and AR6 projections at 2050.

2050 (black lines in Figure 7). The 90% confidence limits are determined using a Monte Carlo simulation with the composite error presented in Figure 6. The 10,000 pairs of perturbed regional rate and acceleration are extrapolated, and the 90% confidence limits are given by the bounds within which 90% of the extrapolations lie (gray shaded area in Figure 7).

10.1029/2024JC022094

Table 1
Future Relative Sea Level (RSL) Change Based on Extrapolated Satellite Altimetry and IPCC AR6 Climate Model Projections of Total RSL Change

Region	ΔRSL from 2020 to 2050 based on extrapolated observations (cm)	90% confidence limit (cm)	Best-fit SSP from the IPCC AR6	ΔRSL from 2020 to 2050 based on the best-fit AR6 SSP (cm)
North Pacific	22	5	5–8.5	19
North Atlantic	19	6	3–7.0	18
South Atlantic	17	4	1–2.6	17
Indian Ocean	15	5	1–2.6	16
South Pacific	14	5	1–2.6	14
Tropical Pacific	13	5	1–2.6	16
Southern Ocean	12	4	1–2.6	12

The observation-based extrapolations are compared with climate model projections of total RSL change from the IPCC AR6 (Fox-Kemper et al., 2021b; Garner et al., 2021; Kopp et al., 2023). No single climate model can compute sea level rise driven by all relevant processes yet, so the IPCC AR6 projections are comprised of seven independent climate models of the different components driving RSL change, each of which is run many times and incorporated in a probabilistic projection of the forced response. The climate models project RSL change driven by (a) glaciers, (b) GrIS, (c) AIS, (d) terrestrial water storage, (e) thermosteric sea level change, (f) dynamic ocean topography and circulation, and (g) GIA plus other drivers of long-term VLM, plus the GRD effects of each of the seven contributing processes (e.g., Table 9.7 in the IPCC AR6 Chapter 9; Fox-Kemper et al., 2021b). We consider only the medium confidence projection data and take the average across quantiles to produce the timseries in Figure 7.

The observation-based extrapolations of RSL fall within the 90% confidence limits of the AR6 projections and have a substantially narrower 90% confidence limit in comparison (Figure 7). Observation-based extrapolations agree better with the high-emissions scenarios (SSP5-8.5 and SSP3-7.0) in the North Pacific and North Atlantic, respectively, but agree better with the low-end emissions scenario (SSP1-2.6) in the remaining regions considered (South Atlantic, Tropical Pacific, South Pacific, Southern Ocean, and Indian Ocean). The results presented in Figure 7 and Table 1 may be used as a guide to select the most appropriate shared socio-economic pathway (SSP) in each region for adaptation and mitigation planning.

Regional dependence of the best-fit SSP scenario (e.g., SSP-5,8.5 in the North Pacific vs. SSP-1,2.6 in the Southern Ocean) indicates that regional variations in the observational record are stronger than those resolved in the AR6 projections (Figure 7). This may indicate that either (a) residual internal variability continues to impact the observational record on a regional scale or (b) the climate models contain errors. With regards to (a), recent work has shown that the strong acceleration in sea level in the U.S. Southeast and Gulf Coast is amplified by internal variability (Dangendorf et al., 2023; Zhang et al., 2024), a region not specifically targeted by the CSEOF modes removed from the MEaSUREs data. However, we emphasize that the North Atlantic region considered here encompasses a much larger area than was studied by Dangendorf et al., or Zhang et al., such that the effects of internal variability are expected to diminish by averaging with the far-North Atlantic where strengthening of the subpolar gyre produces sterodynamic lows (e.g., Karnauskas, 2020). We note that the confidence limits associated with the observation-based extrapolations overlap with multiple AR6 SSP scenarios, indicating that shortcomings in both models and observations are well-encompassed by the uncertainty ranges presented. With regards to (b), climate models are subject to computational limits and therefore require physical approximations (e.g., coarse grid resolution) that may significantly affect the results. Significant overlap within the uncertainty ranges between the two methods confirms that these limitations are not so large as to produce divergent results. Furthermore, the significant overlap between observed and modeled sea level may suggest that the sterodynamic component of sea level is adequately represented in the models despite ice sheets and glaciers not being dynamically coupled to sterodynamic sea level (Fox-Kemper et al., 2021b).

The extrapolated sea level change in 2050 relative to 2020 is listed in Table 1 along with uncertainties and the best-fit SSP from the AR6 projections. The extrapolated sea level rise in 2050 is largest in the North Pacific and

North Atlantic and the main driver is the magnitude of the acceleration in these regions. For example, notice that the present-day rate is largest in the Indian Ocean while the greatest extrapolated value of sea level change arises in the North Pacific. This result highlights the importance of estimating and understanding the acceleration of sea level change on a regional scale.

4. Discussion and Outlook

The results of this study can be summarized as follows: (a) the rate and acceleration of sea level rise have stabilized against the addition of new data in the ocean-basin-scale regions considered (i.e., they appear to be in steady state), which may indicate that the long-term signal driven by climate change has emerged on a regional scale in the observational record; (b) regional variations in the acceleration are particularly large (e.g., standard deviation across the ocean basin scale regions considered is 0.057 mm/year^2 or 69% of the global mean); (c) the strong regional variations in the acceleration produce substantially larger extrapolated RSL rise in the North Pacific and North Atlantic compared to other regions and the global mean in 2050 relative to 2020.

The regional quadratic extrapolations of sea level presented herein are based on the assumption that sea level will continue on the trajectory that has been observed over the past 30 years for the next 30 years. This is the simplest and most conservative assumption that we can make given the complexities of the climate system. The uncertainties we assess provide an estimate of the range within which the trajectory may change, where regional-scale quadratic extrapolations of sea level rise are on the frontier of what is justified based on the 30-year satellite altimeter record. The extrapolations presented herein do not represent the sea level rise expected at each location within a given region but rather the average across the region as a whole. A longer, continuous record of sea level rise will be essential for more refined extrapolations of the observational record, including the consideration of smaller regional scales.

Observation-based extrapolations such as those presented herein provide independent information that can be used to select the most appropriate SSP scenario from the IPCC AR6 total RSL projections. In addition, the uncertainty range of observation-based extrapolated sea level rise is quite narrow compared to the range associated with climate model projection scenarios from the AR6 report. By providing guidance around scenario selection, observation-based extrapolations contribute to reducing uncertainty in expected future sea level rise and the most appropriate response.

Conflict of Interest

The authors declare no conflicts of interest relevant to this study.

Data Availability Statement

The JPL MEaSUREs Gridded Sea Surface Height Anomalies Version 2205 is available for download from https://doi.org/10.5067/SLREF-CDRV3 (Fournier et al., 2022). Software used to produce the Monte Carlo simulation of satellite altimeter measurement errors is available for download from https://doi.org/10.1029/2021EF002290 (Nerem et al., 2022). The medium confidence total relative sea level climate model projections are available for download from https://doi.org/10.5281/zenodo.5914709 (Fox-Kemper et al., 2021a; Garner et al., 2021; Kopp et al., 2023). All scripts and functions used to produce the results presented in this paper are hosted on https://doi.org/10.5281/zenodo.15191354 (Bellas-Manley, 2025).

Acknowledgments

This research was funded by the NASA Sea Level Change Team under Grants 80NSSC21K1191 and 80NSSC25K7226. A big thank you to Lambert Caron for providing the 5,000 member ensemble of GIA models and guidance on quantifying the relevant GIA uncertainty. Thanks to Kris Karnauskas for guidance on regional patterns and ocean dynamics. We thank the AR6 authors and the FACTS team for developing the sea-level rise projections and making them available, multiple funding agencies for supporting the development of the projections, and the NASA Sea Level Change Team for developing and hosting the IPCC AR6 Sea Level Projection Tool. Thanks also to anonymous reviewers for thoughtful comments that greatly improved the manuscript.

References

A, G., Wahr, J., & Zhong, S. (2013). Computations of the viscoelastic response of a 3-D compressible Earth to surface loading: An application to Glacial Isostatic Adjustment in Antarctica and Canada. *Geophysical Journal International*, *192*(2), 557–572. https://doi.org/10.1093/gji/ggs030

Ablain, M., Meyssignac, B., Zawadzki, L., Jugier, R., Ribes, A., Spada, G., et al. (2019). Uncertainty in satellite estimates of global mean sea-level changes, trend and acceleration. *Earth System Science Data*, *11*(3), 1189–1202. https://doi.org/10.5194/essd-11-1189-2019

Adhikari, S., Ivins, E. R., & Larour, E. (2016). ISSM-SESAW v1.0: Mesh-based computation of gravitationally consistent sea-level and geodetic signatures caused by cryosphere and climate driven mass change. *Geoscientific Model Development*, *9*(3), 1087–1109. https://doi.org/10.5194/gmd-9-1087-2016

Bellas-Manley, A. (2025). SeaLevelExtrapolation_2025: V3 [Software]. *Zenodo*. https://doi.org/10.5281/zenodo.15191354

Bos, M. S., Williams, S. D. P., Arajo, I. B., & Bastos, L. (2014). The effect of temporal correlated noise on the sea level rate and acceleration uncertainty. *Geophysical Journal International*, *196*(3), 1423–1430. https://doi.org/10.1093/gji/ggt481

Caron, L., Ivins, E. R., Larour, E., Adhikari, S., Nilsson, J., & Blewitt, G. (2018). GIA model statistics for GRACE hydrology, cryosphere, and ocean science. *Geophysical Research Letters*, *45*(5), 2203–2212. https://doi.org/10.1002/2017GL076644

Dalpadado, P., Roxy, M. K., Arrigo, K. R. , van Dijken, G. L., Chierici, M., Ostrowski, M., et al. (2024). Rapid climate change alters the environment and biological production of the Indian Ocean. *Science of The Total Environment*, *906*, 167342. https://doi.org/10.1016/j.scitotenv.2023.167342

Dangendorf, S., Hendricks, N., Sun, Q., Klinck, J., Ezer, T., Frederikse, T., et al. (2023). Acceleration of U.S. Southeast and Gulf coast sea-level rise amplified by internal climate variability. *Nature Communications*, *14*(1), 1935. https://doi.org/10.1038/s41467-023-37649-9

Diener, T., Sasgen, I., Agosta, C., Fürst, J. J., Braun, M. H., Konrad, H., & Fettweis, X. (2021). Acceleration of dynamic ice loss in Antarctica from satellite gravimetry. *Frontiers in Earth Science*, *9*, 741789. https://doi.org/10.3389/feart.2021.741789

Fasullo, J. T., & Nerem, R. S. (2018). Altimeter-era emergence of the patterns of forced sea-level rise in climate models and implications for the future. *Proceedings of the National Academy of Sciences of the United States of America*, *115*(51), 12944–12949.

Fournier, S., Willis, J., Killett, E., Qu, Z., & Zlotnicki, V. (2022). JPL MEaSUREs gridded sea surface height anomalies version 2205 PO.DAAC. [Dataset]. https://doi.org/10.5067/SLREF-CDRV3

Fox-Kemper, B., Hewitt, H. T., Xiao, C., Aðalgeirsdóttir, G., Drijfhout, S. S., Edwards, T. L., et al. (2021a). Ocean, cryosphere and sea level change [Dataset]. In V. Masson-Delmotte, P. Zhai, A. Pirani, S. L. Connors, C. Péan, S. Berger, et al. (Eds.), *Climate change 2021: The physical science basis. Contribution of working group I to the sixth assessment report of the intergovernmental panel on climate change* (pp. 1211–1362). Cambridge University Press. https://doi.org/10.1017/9781009157896.011

Fox-Kemper, B., Hewitt, H. T., Xiao, C., Aðalgeirsdóttir, G., Drijfhout, S. S., Edwards, T. L., et al. (2021b). Ocean, cryosphere and sea level change. In V. Masson-Delmotte, P. Zhai, A. Pirani, S. L. Connors, C. Péan, S. Berger (Eds.), *Climate change 2021: The physical science basis. Contribution of working group I to the sixth assessment report of the intergovernmental panel on climate change* (pp. 1211–1362). Cambridge University Press. https://doi.org/10.1017/9781009157896.011

Frederikse, T., Riva, R. E. M., & King, M. A. (2017). Ocean bottom deformation due to present-day mass redistribution and its impact on sea level observations. *Geophysical Research Letters*, *44*(24), 12306–12314. https://doi.org/10.1002/2017GL075419

Garner, G. G., Hermans, T., Kopp, R. E., Slangen, A. B. A., Edwards, T. L., Levermann, A., et al. (2021). IPCC AR6 sea level projections. Version 20210809. [Dataset]. https://doi.org/10.5281/zenodo.5914709

Gomez, N. M. Y., Pollard, D., DeConto, R. M., Sadai, S., Lloyd, A., Nyblade, A., et al. (2024). The influence of realistic 3D mantle viscosity on Antarctica's contribution to future global sea levels. *Science Advances*, *10*(31), eadn1470. https://doi.org/10.1126/sciadv.adn1470

Gregory, J. M., Griffies, S. M., Hughes, C. W., Lowe, J. A., Church, J. A., Fukimori, I., et al. (2019). Concepts and terminology for sea level: Mean, variability and change, both local and global. *Surveys in Geophysics*, *40*(6), 1251–1289. https://doi.org/10.1007/s10712-019-09525-z

Gunn, K. L., Rintoul, S. R., England, M. H., & Bowen, M. M. (2023). Recent reduced abyssal overturning and ventilation in the Australian Antarctic Basin. *Nature Climate Change*, *13*(6), 537–544. https://doi.org/10.1038/s41558-023-01667-8

Haigh, I. D., Wahl, T., Rohling, E. J., Price, R. M., Pattiaratchi, C. B., Calafat, F. M., & Dangendorf, S. (2014). Timescales for detecting a significant acceleration in sea level rise. *Nature Communications*, *5*(1), 3635. https://doi.org/10.1038/ncomms4635

Hamlington, B. D., Bellas-Manley, A., Willis, J. K., Fournier, S., Vinogradova, N., Nerem, R. S., et al. (2024). The rate of global sea level rise doubled during the past three decades. *Communications Earth & Environment*, *5*(1), 601. https://doi.org/10.1038/s43247-024-01761-5

Hamlington, B. D., Cheon, S. H., Piecuch, C. G., Karnauskas, K. B., Thompson, P. R., Kim, K.-Y., et al. (2019). The dominant global modes of recent internal sea level variability. *Journal of Geophysical Research: Oceans*, *124*(4), 2750–2768. https://doi.org/10.1029/2018JC014635

Hamlington, B. D., Cheon, S. H., Thompson, P. R., Merrifield, M. A., Nerem, R. S., Leben, R. R., & Kim, K.-Y. (2016). An ongoing shift in Pacific Ocean sea level. *Journal of Geophysical Research: Oceans*, *121*(7), 5084–5097. https://doi.org/10.1002/2016JC011815

Hamlington, B. D., Gardner, A. S., Ivins, E., Lenaerts, J. T. M., Reager, J. T., Trossman, D. S., et al. (2020). Understanding of contemporary regional sea-level change and the implications for the future. *Reviews of Geophysics*, *58*(3), e2019RG000672. https://doi.org/10.1029/2019RG000672

Hamlington, B. D., Leben, R. R., Nerem, R. S., Han, W., & Kim, K.-Y. (2011). Reconstructing sea level using cyclostationary empirical orthogonal functions. *Journal of Geophysical Research*, *116*(C12), C12015. https://doi.org/10.1029/2011JC007529

Hamlington, B. D., Leben, R. R., Strassburg, M. W., & Kim, K. Y. (2014). Cyclostationary empirical orthogonal function sea-level reconstruction. *Geoscience Data Journal*, *1*(1), 13–19. https://doi.org/10.1002/gdj3.6

Hugonnet, R., McNabb, R., Berthier, E., Menounos, B., Nuth, C., Girod, L., et al. (2021). Accelerated global glacier mass loss in the early twenty-first century. *Nature*, *592*(7856), 726–731. https://doi.org/10.1038/s41586-021-03436-z

Ishii, M., Kimoto, M., Sakamoto, K., & Iwasaki, S. I. (2006). Steric sea level changes estimated from historical ocean subsurface temperature and salinity analyses. *Journal of Oceanography*, *62*(2), 155–170. https://doi.org/10.1007/s10872-006-0041-y

Jevrejeva, S., Moore, J. C., Grinsted, A., Matthews, A. P., & Spada, G. (2014). Trends and acceleration in global and regional sea levels since 1807. *Global and Planetary Change*, *113*, 11–22. https://doi.org/10.1016/j.gloplacha.2013.12.004

Karnauskas, K. (2020). *Physical oceanography and climate*. Cambridge University Press.

Kopp, R. E., Garner, G. G., Hermans, T. H. J., Jha, S., Kumar, P., Reedy, A., et al. (2023). The Framework for Assessing Changes To Sea-Level (FACTS) v1.0: A platform for characterizing parametric and structural uncertainty in future global, relative, and extreme sea-level change [Dataset]. *Geoscientific Model Development*, *16*(24), 7461–7489. https://doi.org/10.5194/gmd-16-7461-2023

Kopp, R. E., Hay, C. C., Little, C. M., & Mitrovica, J. X. (2015). Geographic variability of sea-level change. *Current Climate Change Reports*, *1*(3), 192–204. https://doi.org/10.1007/s40641-015-0015-5

Lee, S., L'Heureux, M., Wittenberg, A. T., Seager, R., O'Gorman, P. A., & Johnson, N. C. (2022). On the future zonal contrasts of equatorial Pacific climate: Perspectives from Observations, Simulations, and Theories. *npj Climate and Atmospheric Science*, *5*(1), 82. https://doi.org/10.1038/s41612-022-00301-2

Maul, G. A., & Martin, D. M. (1993). Sea level rise at Key West, Florida, 1846-1992: America's longest instrument record? *Geophysical Research Letters*, *20*, 18–1958. https://doi.org/10.1029/93GL02371

Mitrovica, J. X., Tamisiea, M. E., Davis, J. L., & Milne, G. A. (2001). Recent mass balance of polar ice sheets inferred from patterns of global sea-level change. *Nature*, *409*(6823), 1026–1029. https://doi.org/10.1038/35059054

Nerem, R. S., Frederikse, T., & Hamlington, B. D. (2022). Extrapolating empirical models of satellite-observed global mean sea level to estimate future sea level change [Software] Zenodo. *Earth's Future*, *10*(4). https://doi.org/10.1029/2021EF002290.e2021EF002290.

Otosaka, I. N., Shepherd, A., Ivins, E. R., Schlegel, N.-J., Amory, C., van den Broeke, M. R., et al. (2023). Mass balance of the Greenland and Antarctic ice sheets from 1992 to 2020. *Earth System Science Data*, *15*(4), 1597–1616. https://doi.org/10.5194/essd-15-1597-2023

Paulson, A., Zhong, S., & Wahr, J. (2005). Modelling post-glacial rebound with lateral viscosity variations. *Geophysical Journal International*, *163*(1), 357–371. https://doi.org/10.1111/j.1365-246X.2005.02645.x

Peltier, W. R., Argus, D. F., & Drummond, R. (2015). Space geodesy constrains ice age terminal deglaciation: The global ICE-6G_C (VM5a) model. *Journal of Geophysical Research: Solid Earth*, *120*, 450–487. https://doi.org/10.1002/2014JB011176

Richter, K., Meyssignac, B., Slangen, A. B., Melet, A., Church, J. A., Fettweis, X., et al. (2020). Detecting a forced signal in satellite-era sea-level change. *Environmental Research Letters*, *15*(9), 094079. https://doi.org/10.1088/1748-9326/ab986e

Riva, R. E. M., Frederikse, T., King, M. A., Marzeion, B., & van den Broeke, M. R. (2017). Brief communication: The global signature of post-1900 land ice wastage on vertical land motion. *The Cryosphere*, *11*(3), 1327–1332. https://doi.org/10.5194/tc-11-1327-2017

Rounce, D. R., Hock, R., Maussion, F., Hugonnet, R., Kochtitzky, W., Huss, M., et al. (2023). Global glacier change in the 21st century: Every increase in temperature matters. *Science*, *379*(6627), 78–83. https://doi.org/10.1126/science.abo1324

Royston, S., Watson, C. S., Legresy, B., King, M. A., Church, J. A., & Bos, M. S. (2018). Sea-level trend uncertainty with Pacific climatic variability and temporally-correlated noise. *Journal of Geophysical Research: Oceans*, *123*(3), 1978–1993. https://doi.org/10.1002/2017jc013655

Seager, R., & Simpson, I. R. (2016). Western boundary currents and climate change. *Journal of Geophysical Research: Oceans*, *121*, 7212–7214. https://doi.org/10.1002/2016JC012156

Slangen, A. B. A., Carson, M., Katsman, C. A., van de Wal, R. S. W., Köhl, A., Vermeersen, L. L. A., & Stammer, D. (2014). Projecting twenty-first century regional sea-level changes. *Climatic Change*, *124*(1–2), 317–332. https://doi.org/10.1007/s10584-014-1080-9

Stammer, D., Cazenave, A., Ponte, R. M., & Tamisiea, M. E. (2013). Causes for contemporary regional sea-level changes. *Annual Review of Marine Science*, *5*(1), 21–46. https://doi.org/10.1146/annurev-marine-121211-172406

Strassburg, M. W., Hamlington, B. D., Leben, R. R., & Kim, K. Y. (2014). A comparative study of sea level reconstruction techniques using 20 years of satellite altimetry data. *Journal of Geophysical Research: Oceans*, *119*(7), 4068–4082. https://doi.org/10.1002/2014JC009893

Sweet, W. V., Kopp, R. E., Weaver, C. P., Obeysekera, J., Horton, R. M., Thieler, E. R., & Zervas, C. (2017). *Global and regional Sea Level rise scenarios for the United States*. NOAA Technical Report NOS CO-OPS 083. NOAA/NOS Center for Operational Oceanographic Products and Services.

Tamisiea, M. E. (2011). Ongoing glacial isostatic contributions to observations of sea level change. *Geophysical Journal International*, *186*(3), 1036–1044. https://doi.org/10.1111/j.1365-246X.2011.05116.x

Ummenhofer, C. C., Murty, S. A., Sprintall, J., Lee, T., & Abram, N. J. (2021). Heat and freshwater changes in the Indian Ocean region. *Nature Reviews Earth & Environment*, *2*(8), 525–541. https://doi.org/10.1038/s43017-021-00192-6

Velicogna, I., Mohajerani, Y., A, G., Landerer, F., Mouginot, J., Noel, B., et al. (2020). Continuity of ice sheet mass loss in Greenland and Antarctica from the GRACE and GRACE Follow-On missions. *Geophysical Research Letters*, *47*(8), e2020GL087291. https://doi.org/10.1029/2020GL087291

Vishwakarma, B. D., Royston, S., Riva, R. E. M., Westaway, R. M., & Bamber, J. L. (2020). Sea level budgets should account for ocean bottom deformation. *Geophysical Research Letters*, *47*(3), e2019GL086492. https://doi.org/10.1029/2019GL086492

Wiese, D. N., Yuan, D.-N., Boening, C., Landerer, F. W., & Watkins, M. M. (2023). JPL GRACE and GRACE-FO Mascon Ocean, Ice, and Hydrology Equivalent Water Height CRI Filtered. *Ver. RL06.1Mv03. PO.DAAC, CA, USA*. https://doi.org/10.5067/TEMSC-3JC63

Yang, H., Lohmann, G., Lu, J., Gowan, E. J., Shi, X., Liu, J., & Wang, Q. (2020). Tropical expansion driven by poleward advancing midlatitude meridional temperature gradients. *Journal of Geophysical Research: Atmospheres*, *125*(16), e2020JD033158. https://doi.org/10.1029/2020JD033158

Yang, H., Lohmann, G., Wei, W., Dima, M., Ionita, M., & Liu, J. (2016). Intensification and poleward shift of subtropical western boundary currents in a warming climate. *Journal of Geophysical Research: Oceans*, *121*, 4928–4945. https://doi.org/10.1002/2015JC011513

Zhang, L., Delworth, T. L., Yang, X., Zeng, F., Gu, Q., & Li, S. (2024). Causes and multiyear predictability of the rapid acceleration of U.S. Southeast Sea level rise after 2010. *npj Climate and Atmospheric Science*, *7*(1), 113. https://doi.org/10.1038/s41612-024-00670-w